Defect and Diffusion Forum
ISSN: 1662-9507, Vol. 451, pp 55-62
doi:10.4028/p-Dcjc3i

Submitted: 2026-01-07
Revised: 2026-02-26
Accepted: 2026-03-01
Online: 2026-04-17

3D-Printed Pyrography Using PLA/Wood Filaments

Francisco Comino[1,a,*], José A. Martínez-Sánchez[1,b], Alessandro Pellegrini[2,c], Roberto Spina[3,4,5,d]

[1]Departamento de Mecánica, Universidad de Córdoba, Spain

[2]Dip. di Scienze Agrarie, Alimenti, Risorse Naturali e Ingegneria (DAFNE), Università di Foggia, Italy

[3]Dip. di Meccanica, Matematica e Management (DMMM), Politecnico di Bari, Italy

[4]Istituto Nazionale di Fisica Nucleare (INFN) - Sezione di Bari, Italy

[5]Consiglio Nazionale delle Ricerche - Istituto di Fotonica e Nanotecnologie (CNR-IFN), Italy

[a]francisco.comino@uco.es, [b]z12masaj@uco.es, [c]alessandro.pellegrini@unifg.it, [d]roberto.spina@poliba.it ([*]corresponding author)

Keywords: Composite, 3D pyrography, Wood filament, Material Extrusion.

Abstract. Wood-filled PLA filaments enable 3D pyrography in material-extrusion (MEX) printing, in which tonal gradients and surface shading are generated in situ by controlling the thermal history during deposition, thereby avoiding post-processing or multi-material strategies. This enables the direct embedding of motifs and graded shading for customized product design, while also allowing appearance stabilization for repeatable manufacturing of wood-filled PLA parts. In this work, PLA/olive-wood (OW) composite filaments containing 0-20 wt.% OW (particle size < 180 μm) were manufactured and printed into 20 mm discs using MEX. The extrusion (nozzle) temperature was varied from 180 to 280 °C, and the printing speed was set to 20 and 200 mm/s to modulate thermal exposure. Surface color was quantified as L^*, a^*, b^* from visible absorbance measurements (400-700 nm) converted into CIELAB coordinates. Percentual differences were assessed using the CIEDE2000 metric ΔE_{00}. The results demonstrated that increasing nozzle temperature progressively reduced lightness L^*, and under severe conditions, a marked loss of chroma (a^* and b^*), particularly for higher OW contents. Low-speed printing (20 mm/s) amplified the pyrographic effect, reaching strong perceptual contrasts (maximum $\Delta E_{00} \approx 9$ at 280 °C for 20 wt.% OW), whereas high-speed printing (200 mm/s) mitigated extreme darkening and maintained more moderate, controlled color differences (typically $\Delta E_{00} < 3$). Accordingly, ΔE00< 3 can be used as a practical "color-stable" target for uniform-looking parts, whereas ΔE00= 3-9 provides clearly distinguishable shades for pyrographic marking/shading. These findings defined practical process windows to either maximize tonal contrast for 3D pyrography or stabilize the appearance for consistent manufacturing of PLA/OW parts.

Introduction

Material Extrusion (MEX) additive manufacturing has evolved from rapid prototyping toward design-oriented manufacturing due to its geometric freedom, short lead times, and efficient material usage. Among thermoplastics, polylactic acid (PLA) has become a benchmark material in MEX due to its bio-based origin and relatively high printability [1].

In parallel, efforts to reduce the environmental impact of polymer products have promoted the development of PLA composites reinforced with lignocellulosic fillers (wood flour/fibers and agroforestry by-products), which can lower costs and embodied energy while providing a natural appearance and tactile quality [1,2]. When incorporated into filaments for MEX, these fillers can be processed successfully if particle size and moisture are adequately controlled, however, their addition often introduces interfacial and rheological challenges (e.g., voids, fiber pull-out, rougher surfaces), strengthening the need to understand the process–structure–surface relationship in printed parts [3,4]. Within this context, olive-wood (OW) residues are especially relevant in Mediterranean regions,

where the olive sector generates large volumes of low-value by-products, and additional streams arise from the removal of trees affected by *Xylella fastidiosa* [5]. Combining OW with PLA strongly promotes circular-economy strategies by valorizing locally available biomass residues in a bio-based polymer matrix.

From a manufacturing perspective, nozzle (extrusion) temperature is one of the key levers in MEX, as it governs melt stability and interlayer bonding. It also accelerates thermo-oxidative reactions that can alter both surface texture and visual appearance, thereby minimizing post-processing while maintaining controlled, in-process outcomes, thereby reducing additional energy/material use and process steps [6]. Beyond traditional functional applications of PLA/wood in MEX (e.g., functional prototypes, acoustic panels, and heat- and mass-exchange devices), there is growing interest in exploiting process-material interactions to introduce new functionalities and aesthetic functions directly during printing [7,8]. One emerging example is 3D pyrography, in which increasing extrusion temperature can induce degradation and partial carbonization of the wood fraction, produce a broad palette of shades (from light to dark), and enable the direct embedding of motifs, gradients, or surface markers during printing, without requiring multi-material approaches [9]. In practice, this can be exploited to embed logos, lettering, serial numbers, and QR-like markers, or to create controlled gradients for product personalization and traceability. This process is attractive for customized product design and surface-embedded information, but it requires defining robust parameter windows that translate deposition conditions into predictable optical outputs. Although prior studies have demonstrated the printability of PLA/wood filaments and reported the influence of processing on morphology and surface quality, material-specific frameworks that simultaneously connect thermal constraints, surface texture, and quantitative color development remain limited, particularly for PLA/OW systems [10,11]. Likewise, while data-driven monitoring and diagnosis approaches have been proposed for MEX to improve quality assurance, these are rarely linked to practical, design-oriented maps of surface texture and optical response for wood-filled PLA.

Therefore, the present study provides a PLA/OW-specific, reproducible route to process-controlled 3D pyrography supported by objective color metrics. The main objective is to establish 3D pyrography as an in-process optical functionality in MEX-printed PLA/OW parts by (i) manufacturing PLA/OW filaments (0-20 wt.% OW) from pruning residues, (ii) quantifying optical appearance through visible spectroscopy converted into CIELAB coordinates (L^*, a^*, b^*) and the perceptual difference ΔE_{00} [13], and (iii) evaluating how extrusion temperature (180-280 °C) and printing speed (20-200 mm/s) govern the achievable tonal range and color stability.

To link the quantitative metrics to practical use, two representative application envelopes are considered: (i) appearance-stable manufacturing, where the goal is to keep deviations limited (e.g., $\Delta E00 \leq 3$ and small shifts in L, a, and b* relative to the reference tone of each formulation), and (ii) intentional pyrographic marking and shading, where clearly distinguishable tones are required (e.g., $\Delta E00 \geq 3$, with strong contrasts typically $\Delta E00 \approx 5–9$).

Materials and Methods

Polylactic acid (PLA) Luminy LX175 (TotalEnergies Corbion, The Netherlands) was selected as the polymer matrix. Olive-wood (OW) particles were obtained as a by-product of pruning, then milled and sieved to a particle size below 180 μm to ensure stable filament extrusion and minimize clogging during material extrusion (MEX). Five formulations were prepared: neat PLA, PLA/OW05 (5 wt.% OW), PLA/OW10 (10 wt.% OW), PLA/OW15 (15 wt.% OW), and PLA/OW20 (20 wt.% OW). Before compounding, PLA pellets and OW particles were oven-dried at 60 °C for 12 h to reduce residual moisture below 2 wt.% and limit hydrolytic degradation and bubble formation during melt processing. PLA pellets were ground into powder to improve mixing with the lignocellulosic filler. Composite blends were prepared by gravimetric dosing and compounded in a co-rotating twin-screw extruder using a temperature profile of 170-190-200 °C. The extrudate was strand-cooled in a water bath and pelletized. Composite pellets were subsequently converted into filaments using a single-screw extruder (L/D = 24) equipped with temperature control and an in-line laser diameter gauge. A 170-200 °C profile and a screw speed of 60 rpm were used, with extrusion through a 2 mm die and

cooling in dual water baths. Filaments were drawn using a traction system to achieve a nominal diameter of 1.75 ± 0.03 mm, suitable for MEX printers.

Disc specimens (20 mm diameter) were manufactured using an X1C MEX printer (Bambu Lab, China). The printing settings were kept constant, as shown in Table 1. The X1C hotend is rated up to 300 °C. However, 280 °C was selected as a conservative upper bound for PLA/OW to limit excessive thermal degradation and potential nozzle fouling while still reaching the strongest controlled pyrographic contrasts. To investigate the 3D pyrography response, nozzle temperature *T* and printing speed *V* were varied within 180-280 °C and 20-200 mm/s, respectively, while the remaining parameters were kept constant.

Table 1. Printing parameters.

Parameter	Value
Layer height	0.2 mm
Layer width	0.4 mm
Raster angle	45 º
Infill density (line pattern)	100 %
Build plate temperature	65 °C
Build orientation	Horizontal (*XY*)

Visible absorbance spectra were measured in the 400-700 nm range using a NIRSystems DS2500 spectrometer (FOSS, Denmark) on the printed discs. From the measured absorbance spectrum data $A(\lambda)$, the spectral reflectance $R(\lambda)$ was obtained using the diffuse-reflectance absorbance definition (Eq. 1).

$$A(\lambda) = \log_{10}\left(\frac{1}{R(\lambda)}\right) \rightarrow R(\lambda)=10^{A(\lambda)} \tag{1}$$

CIELAB coordinates were computed following CIE recommendations by first calculating the tristimulus values (X,Y,Z) through discrete integration of R(λ) weighted by the spectral power distribution of Illuminant A and the CIE 1931 2° standard observer color-matching functions $\overline{x}(\lambda)$, $\overline{y}(\lambda)$, $\overline{z}(\lambda)$, see Eq. 2, 3, and 4. A spectral step of $\Delta(\lambda)$=0.5 nm was used.

$$X=k\sum_{\lambda} R(\lambda)\, S_A(\lambda)\, \overline{x}(\lambda)\, \Delta\lambda \tag{2}$$

$$Y=k\sum_{\lambda} R(\lambda)\, S_A(\lambda)\, \overline{y}(\lambda)\, \Delta\lambda \tag{3}$$

$$Z=k\sum_{\lambda} R(\lambda)\, S_A(\lambda)\, \overline{z}(\lambda)\, \Delta\lambda \tag{4}$$

The normalization factor *k* (Eq. 5) was defined so that the reference white under the same observer conditions satisfies $Y_n = 100$.

$$K = \frac{100}{\sum_{\lambda} S_A(\lambda)\, \overline{y}(\lambda)\, \Delta\lambda} \tag{5}$$

CIELAB coordinates L^*, a^*, b^* were then computed using the reference tristimulus values (X_n, Y_n, Z_n) of the perfect reflecting diffuser, see Eq. 6, 7, and 8.

$$L^*=116 \cdot f\left(\frac{Y}{Y_n}\right)\text{-}16 \tag{6}$$

$$a^*=500 \cdot \left[f\left(\frac{X}{X_n}\right)-f\left(\frac{Y}{Y_n}\right)\right] \quad (7)$$

$$b^*=200 \cdot \left[f\left(\frac{Y}{Y_n}\right)-f\left(\frac{Z}{Z_n}\right)\right] \quad (8)$$

with the standard non-linear function:

$$f(t)=\begin{cases} t^{1/3} & t>\delta^3 \\ \frac{t}{3\delta^2}+\frac{4}{29} & t \le \delta^3 \end{cases} \quad where\ \delta=\frac{6}{29} \quad (9)$$

This workflow yielded objective color descriptors (lightness L^*, red–green a^*, and yellow–blue b^*) suitable for quantifying process-induced pyrographic tonal changes.

To quantify perceptual color differences, the CIEDE2000 total color difference was computed for each specimen relative to its reference condition (printed at 180 °C and 20 mm/s for each material), as shown in Eq. 10. Under reference viewing conditions, the parametric factors were set to $k_L = k_C = k_H = 1$.

$$\Delta E_{00}=\sqrt{\left(\frac{\Delta L'}{k_L S_L}\right)^2+\left(\frac{\Delta C'}{k_C S_C}\right)^2+\left(\frac{\Delta H'}{k_H S_H}\right)^2+R_T\left(\frac{\Delta C'}{k_C S_C}\right)\left(\frac{\Delta H'}{k_H S_H}\right)} \quad (10)$$

Results and Discussion

The 3D pyrography effect was assessed by converting the measured visible absorbance spectra to CIELAB coordinates (L^*, a^*, b^*) and then computing the perceptual color difference (CIEDE2000) relative to the reference condition (180 °C, 20 mm/s) for each formulation. The influence of extrusion temperature (180-280 °C), printing speed (20 and 200 mm/s), and olive-wood (OW) content (5-20 wt.%) is discussed below.

For interpretation, ΔE00 is used as the primary design metric: ΔE00≲ 1 is typically imperceptible, ΔE00≈ 1-3 corresponds to slight-to-moderate differences, and ΔE00≳ 3 to clearly noticeable differences. Accordingly, the "appearance-stable" regime is associated with ΔE00≤ 3 (limited variations in L*, a*, b* around the reference tone of each formulation), whereas intentional pyrographic marking and shading targets ΔE00≥ 3, with strong contrasts at ΔE00≈ 5-9.

The variation of the L^* parameter with respect to extrusion temperature and speed for each composite is shown in Fig. 1. Extrusion temperature was the primary driver of lightness variation, with printing speed acting as a potent modulator of the thermal "pyrographic" outcome. At 20 mm/s (solid lines), L^* was relatively stable between 180 and 260 °C for most formulations, but a pronounced darkening occurred at 280 °C, particularly for high OW contents. PLA/OW15 and PLA/OW20 drop to $L^* \approx 24$, indicating a significant tonal change toward darker surfaces. In contrast, PLA/OW05 decreased slightly across the entire temperature range, whereas PLA/OW10 exhibited the smallest overall L^* reduction, suggesting a lower sensitivity of lightness to extreme thermal exposure.

At 200 mm/s (dashed lines), L^* values were consistently higher and less sensitive to temperature, mainly remaining within a narrower band even at 280 °C. This outcome indicated that high printing speed mitigated excessive darkening, consistent with a reduced thermal history during deposition (i.e., a shorter residence time at elevated temperature). Overall, the combination of high temperature and low speed produced the most significant decrease in L^*, whereas high speed promoted lightness stability.

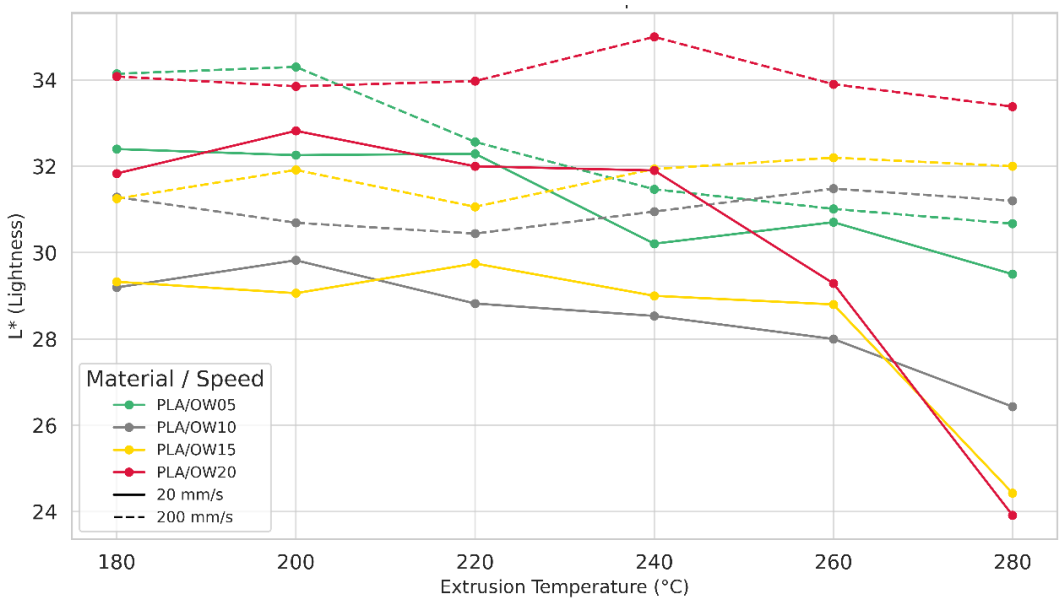

Fig. 1. Variation of L^* as a function of extrusion temperature and printing speed.

The a^*-b^* chromaticity map (Fig. 2) provides insight into how hue and chroma evolve beyond simple darkening. Most conditions clustered in the region of positive a^* and positive b^* (reddish/yellowish tones), typical of wood-filled thermoplastics. For moderate temperatures (approximately 180-260 °C), points tended to remain in this quadrant with relatively limited dispersion, indicating that color changes were dominated by gradual shifts rather than abrupt hue inversion. However, under the most severe processing condition (280 °C, 20 mm/s), the higher-OW materials exhibited pronounced migration toward lower a^* and much lower b^* (i.e., loss of redness and yellowness). This pronounced reduction in chroma was consistent with substantial thermal darkening, where the surface appearance became less saturated and more burnt-like. At 200 mm/s, the corresponding points remained closer to the central cluster, again supporting that fast deposition limited the extent of thermally induced discoloration.

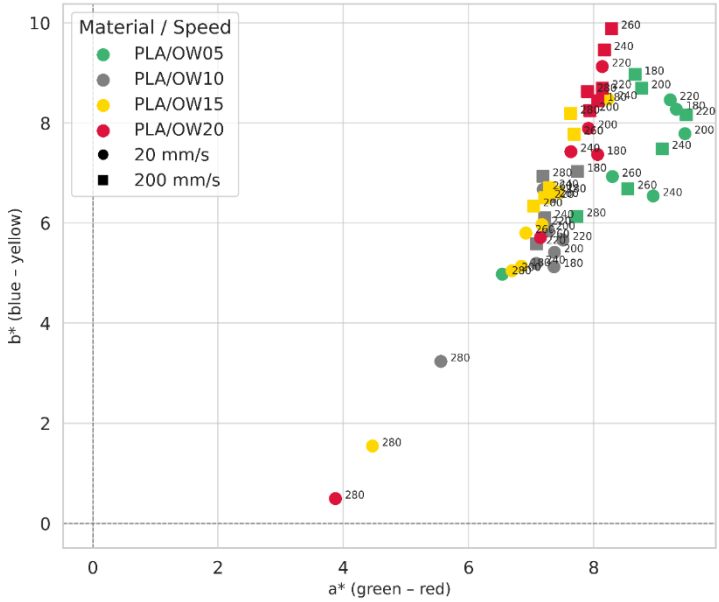

Fig. 2. CIELAB chromaticity plot (a^* vs. b^*) as a function of extrusion temperature and printing speed.

Fig. 3 reports ΔE_{00} as a function of extrusion temperature, ranging from 20 mm/s to 200 mm/s, using 180 °C and 20 mm/s as the reference for each formulation. At 20 mm/s (Fig. 3a), ΔE_{00} remained

low at 200-220 °C (typically ≤ 1.36 depending on formulation), indicating minor deviations from the reference tone. As the temperature increased, the response became formulation-dependent and clearly nonlinear, with the most significant changes occurring at 280 °C, where ΔE_{00} reached 4.02 (PLA/OW05), 3.08 (PLA/OW10), 5.23 (PLA/OW15), and up to 9.04 (PLA/OW20). This trend confirmed that high OW content, combined with high temperature and low speed, produced the strongest perceptual contrast, which was desirable when intentional tonal variation was required (pyrographic shading).

At 200 mm/s (Fig. 3b), ΔE_{00} variations were moderate across the whole temperature range, mostly between ~0.24 and ~3.17. Because the reference was set at 20 mm/s, the cells at 180 °C were not zero and already exhibited noticeable color shift $\Delta E_{00} \approx 1.70$-2.21, demonstrating that printing speed alone could produce a noticeable color shift even without temperature changes. With increasing temperature, the highest ΔE_{00} values remained limited with respect to 20 mm/s. PLA/OW15 reached 3.07-3.17 at 260-280 °C, whereas PLA/OW20 showed its maximum around 3.01 at 240 °C and then decreased to 1.63 at 280 °C. This behavior indicated that at high speeds, thermal exposure was insufficient to induce extreme darkening, and the resulting color differences remained within a controlled mid-range envelope.

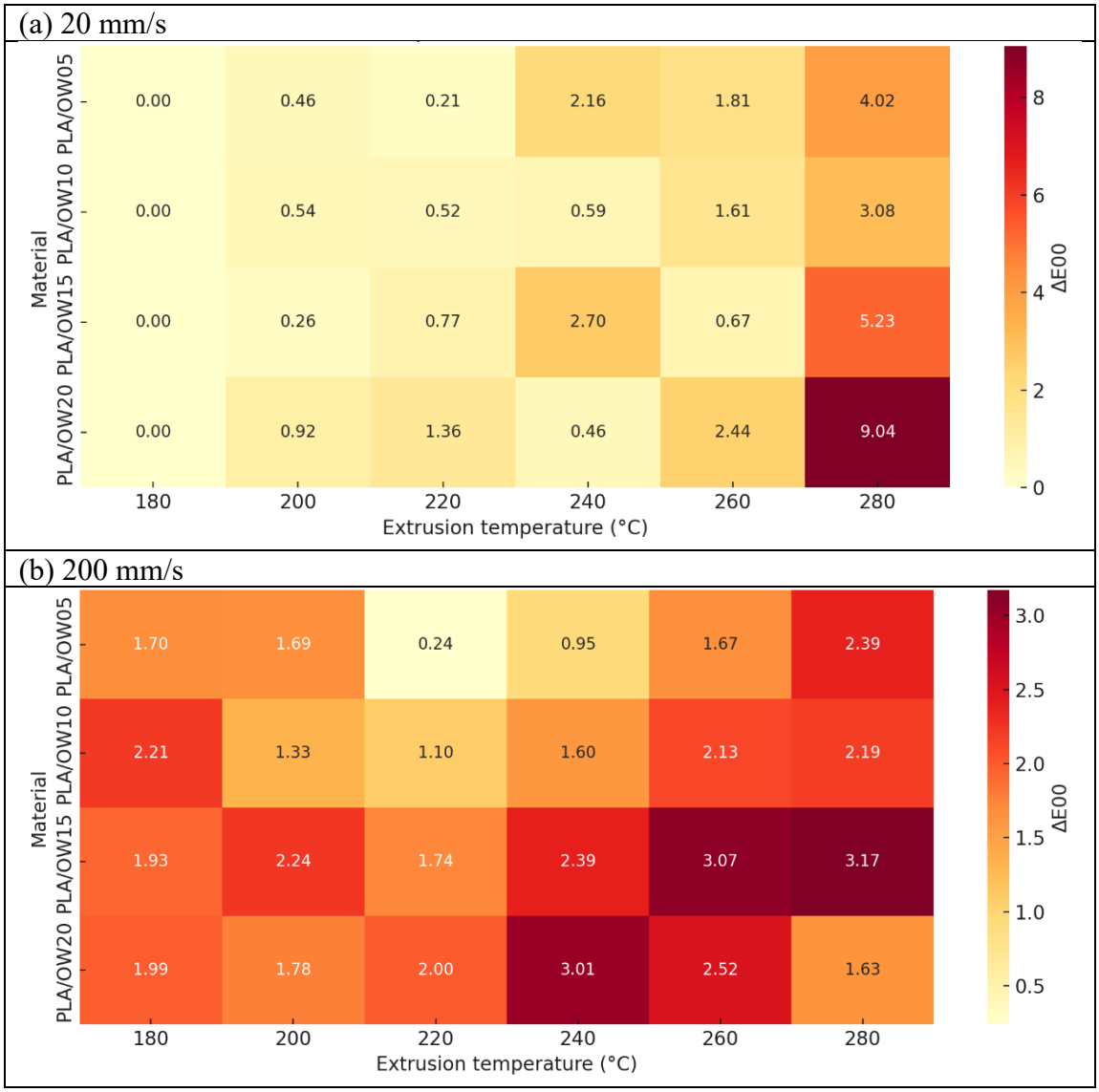

Fig. 3. CIELAB ΔE_{00} as a function of extrusion temperature.

Analysis of all responses (L^*, a^*, b^*, and ΔE_{00}) indicated that the 3D pyrography effect could be tuned by controlling the thermal input during deposition. Low speed increased thermal exposure and amplified thermally driven discoloration, particularly at very high nozzle temperatures and higher

OW contents, where both lightness reduction L^* and chroma loss a^*-b^* became pronounced. On the contrary, high speed reduced the severity of these changes, stabilizing L^* and keeping ΔE_{00} within a moderate range. These results established two practical operating regimes for wood-filled PLA: (i) a contrast-enhancing regime (high temperature + low speed) to maximize tonal variation, and (ii) a color-stabilization regime (high speed, moderate temperature) to minimize unintended darkening while retaining a consistent appearance.

Conclusions

PLA/olive-wood (OW) composite filaments (5–20 wt.% OW) enabled in-process 3D pyrography in material-extrusion printing, where surface tonality can be tuned without post-processing by adjusting deposition conditions.

Color was objectively quantified from visible spectra through the CIELAB coordinates (L^*, a^*, b^*), and the perceptual metric ΔE_{00}. Extrusion temperature produced the most substantial tonal shifts: increasing temperature generally promoted darkening (lower L^*) and, under severe conditions, a loss of chroma (changes in a^* and b^*). Printing speed served as a practical thermal-exposure lever: low speed (20 mm/s) amplified the pyrographic effect and maximized contrast - especially at high temperatures and higher OW content - while high speed (200 mm/s) mitigated extreme darkening and kept ΔE_{00} within a more moderate and controlled range.

Overall, the results demonstrate that PLA/OW composites provided a simple, single-material route to embed shades, gradients, and surface markers directly during printing, while supporting circular-economy valorization of olive-wood residues as a functional filler in sustainable MEX manufacturing.

Acknowledgments

The authors acknowledge financial support from the European Innovation Association (AEI) for agricultural productivity and sustainability, for the creation and operation of operational groups, and from the Ministry of Agriculture, Livestock, Fisheries, and Sustainable Development of the Junta de Andalucía through the research project AGROSEC (reference GOPO-JA-23). The Project was also funded by the Department of Excellence - Law number 232/2016 (Grant No. CUP - D93C23000100001) and Space It Up project funded by the Italian Space Agency, ASI, and the Italian Ministry of University and Research (MUR) under contract n. 2024-5-E.0 (Grant N. CUP-I53D24000060005). They would also like to acknowledge Smart Materials 3D for providing materials.

References

[1] B. Redwood, F. Schöffer, B. Garret, The 3D Printing Handbook, 3D Hubs B.V., Amsterdam, 2018.

[2] Y. Tao, H. Wang, Z. Li, P. Li, S.Q. Shi, Development and application of wood flour-filled polylactic acid composite filament for 3d printing, Materials 10 (2017). https://doi.org/10.3390/ma10040339.

[3] F. Comino, J.A. Martinez-Sánchez, P.E. Romero, N. Gurrado, R. Spina, Thermo-mechanical properties of polylactic acid/olive wood composite for additive manufacturing, in: Materials Research Proceedings, Association of American Publishers, 2025: pp. 2344–2351. https://doi.org/10.21741/9781644903599-253.

[4] N. V. dos Santos, D.K.K. Cavalcanti, J.S.S. Neto, H.F.M. de Queiroz, M.D. Banea, D.C.T. Cardoso, Analysis of voids, interfacial and thermal properties of additively manufactured continuous natural fiber-reinforced biocomposites, Progress in Additive Manufacturing 10 (2025) 5401–5422. https://doi.org/10.1007/s40964-024-00913-5.

[5] A.D. Syanatha, R.A. Setiawan, S. Steven, Y. Mardiyati, Effect of manau rattan (Calamus manan miq.) particle size on processability and mechanical properties of 3D-printed PP/rattan WPC filaments, Progress in Additive Manufacturing 10 (2025) 5387–5399. https://doi.org/10.1007/s40964-024-00912-6.

[6] M. Saponari, A. Giampetruzzi, G. Loconsole, D. Boscia, P. Saldarelli, Xylella fastidiosa in olive in apulia: Where we stand, Phytopathology 109 (2019). https://doi.org/10.1094/PHYTO-08-18-0319-FI.

[7] E. Petinakis, X. Liu, L. Yu, C. Way, P. Sangwan, K. Dean, S. Bateman, G. Edward, Biodegradation and thermal decomposition of poly(lactic acid)-based materials reinforced by hydrophilic fillers, Polym Degrad Stab 95 (2010) 1704–1707. https://doi.org/10.1016/j.polymdegradstab.2010.05.027.

[8] D.D.C.V. Sheng, M.N. Bin Yahya, N.B.C. Din, K.Y. Wong, M.R.M. Asyraf, V. Sekar, Potential of wood fiber/polylactic acid composite microperforated panel for sound absorption application in indoor environment, Constr Build Mater 444 (2024). https://doi.org/10.1016/j.conbuildmat.2024.137750.

[9] F. Comino, P.E. Romero, E. Molero, M. Ruiz de Adana, Experimental evaluation of a 3D printed air dehumidification system developed with green desiccant materials, Appl Therm Eng (2023) 120393. https://doi.org/10.1016/j.applthermaleng.2023.120393.

[10] K. (Justin) Moon, J. Yi, V. Savage, A. Bianchi, 3D printed pyrography: Using wood filament and dynamic control of nozzle temperature for embedding shades of color in objects, Addit Manuf 83 (2024). https://doi.org/10.1016/j.addma.2024.104064.

[11] M. Kariz, M. Sernek, M. Obućina, M.K. Kuzman, Effect of wood content in FDM filament on properties of 3D printed parts, Mater Today Commun 14 (2018) 135–140. https://doi.org/10.1016/j.mtcomm.2017.12.016.

[12] R. Spina, Surface appearance of poly lactic acid due to variations in material extrusion processing parameters, Sci Rep 15 (2025). https://doi.org/10.1038/s41598-025-14484-0.